

# Structural investigation of the carbon deposits on Ni/Al<sub>2</sub>O<sub>3</sub> catalyst modified by CaO-MgO for the biogas dry reforming reaction.

Nikolaos D. Charisiou<sup>1</sup>, Georgios I. Siakavelas<sup>1</sup>, Victor Sebastian<sup>2</sup>, Steven J. Hinder<sup>3</sup>, Mark A. Baker<sup>3</sup>, Vagelis G. Papadakis<sup>4</sup>, Wen Wang<sup>5</sup>, Kyriaki Polychronopoulou<sup>6,7</sup>, Maria A. Goula<sup>1\*</sup>

<sup>1</sup> Laboratory of Alternative Fuels and Environmental Catalysis (LAFEC), Department of Chemical Engineering, University of Western Macedonia, GR-50100, Greece

<sup>2</sup> Chemical and Environmental Engineering Department, Instituto de Nanociencia de Aragón (INA) and Instituto de Ciencia de Materiales de Aragón (ICMA), Universidad de Zaragoza-CSIC, 50018 Zaragoza, Spain

<sup>3</sup> The Surface Analysis Laboratory, Faculty of Engineering and Physical Sciences, University of Surrey, Guildford, GU2 4DL, UK

<sup>4</sup> Department of Environmental Engineering, University of Patras, Agrinio, Greece

<sup>5</sup> Biomass Energy and Environmental Engineering Research Center, Beijing University of Chemical Technology, Beijing 100029, China

<sup>6</sup> Center for Catalysis and Separation, Khalifa University of Science and Technology, Abu Dhabi, P.O. Box 127788, UAE

<sup>7</sup> Department of Mechanical Engineering, Khalifa University of Science and Technology, Abu Dhabi, P.O. Box 127788, UAE

† Presented at the 1st International Electronic Conference on Catalysis Sciences, 10–30 November 2019; Available online: <https://sciforum.net/conference/ECCS2020>

Published: 9 November 2019

**Abstract:** Ni/Al<sub>2</sub>O<sub>3</sub> and Ni/CaO-MgO-Al<sub>2</sub>O<sub>3</sub> catalysts were investigated for the biogas dry reforming reaction using CH<sub>4</sub>/CO<sub>2</sub> mixtures with minimal dilution. Stability tests were carried out between 600 and 800°C and BET, TGA/DTG, Raman, STEM-HAADF, HR-TEM, XPS techniques were used to characterize the carbon deposition on the spent samples. Graphitized carbon allotrope structures, carbon nanotubes and amorphous carbon were formed on all samples. Metallic Ni<sup>0</sup> was recorded for all, whereas a strong peak corresponding to Ni<sub>2</sub>O<sub>3</sub>/NiAl<sub>2</sub>O<sub>4</sub> was observed for the Ni/Al<sub>2</sub>O<sub>3</sub> sample. Stability tests confirmed that the Ni/CaO-MgO-Al<sub>2</sub>O<sub>3</sub> catalyst deactivates at a more gradual rate and is more active and selective in comparison to the Ni/Al<sub>2</sub>O<sub>3</sub> for all temperatures. It was concluded that doping Al<sub>2</sub>O<sub>3</sub> with CaO-MgO enhances catalytic performance by: (a) maintaining the Ni<sup>0</sup> phase during the reaction, due to higher dispersion and stronger active phase-support interactions, (b) leading to a less graphitic and more defective type of deposited carbon, and (c) facilitating the deposited carbon gasification due to the enhanced CO<sub>2</sub> adsorption on its increased surface basic sites.

**Keywords:** biogas dry reforming; syngas production; nickel catalysts; catalytic deactivation; carbon nanotubes; CaO-MgO doping

## 1. Introduction

Biogas is a product of the anaerobic digestion of biomass. It contains mainly CH<sub>4</sub> and CO<sub>2</sub> and can be used for the production of syngas (H<sub>2</sub>/CO) via dry reforming (BDR) [1]. Syngas is a key chemical feedstock for the synthesis of oxygenated chemicals and hydrocarbons via the Fisher-Tropsch process [2]. The major issue that must be overcome when using cheap Ni based systems is carbon deposition on the catalyst surface, which is produced via methane decomposition and carbon monoxide disproportionation. The carbon deposited on the catalyst surface can differ in

nature and structure [3-5]. It is generally accepted that catalytic activity depends on the nature of the support, active phase, synthesis method and pretreatment. Metal oxides such as  $\text{Al}_2\text{O}_3$ ,  $\text{SiO}_2$ ,  $\text{La}_2\text{O}_3$ ,  $\text{CeO}_2$  and  $\text{ZrO}_2$  have been used as supports for Ni based catalysts [6-8], and lanthanide metals (e.g., La, Ce, Pr) [9] or alkaline earth metals (e.g., Sr, Ca, Ba) [11,12] as promoters. The present work reports on the catalytic performance of Ni/Al and Ni/CaO-MgO-Al (Ni/modAl) catalysts using  $\text{CH}_4/\text{CO}_2$  mixtures with minimal dilution, focusing on the correlation between catalytic deactivation and quantity and/or quality of deposited carbon, as a function of time. To this purpose, we conducted a number of stability tests at different reaction temperatures and employed various characterization techniques in order to investigate the coke deposited on the spent catalysts and also to monitor the evolution of Ni oxidation states with the reaction conditions.

## 2. Materials and Methods

### 2.1. Catalyst preparation

The alumina support was obtained from Akzo and the modified alumina (4.5% CaO, 1% MgO, 0.5%  $\text{SiO}_2$ ) by Saint Gobain NorPro in pellet form. The supports were crashed and sieved to 350-500  $\mu\text{m}$  and calcined at 800°C for 4 h. The catalysts were prepared via the wet impregnation technique using the appropriate  $\text{Ni}(\text{NO}_3)_2 \cdot 6\text{H}_2\text{O}$  solution to give catalysts with a Ni content of 8 wt%. The catalysts were dried at 120°C for 12 h, calcined in atmosphere at 800°C for 4 h and in-situ activated for 1 h at 800°C under pure  $\text{H}_2$  flow. The catalysts are denoted as Ni/Al and Ni/modAl.

### 2.2. Materials characterization

For the spent catalysts the amount of carbon deposited was measured with a thermogravimetric analyzer (TGA), on a Leco TGA 701 instrument. The coke deposited on the spent catalytic samples was also characterized by Raman spectroscopy. For each sample, at least three Raman spectra were collected in different areas to assess the homogeneity of the investigated material. Transmission electron microscopy (TEM) measurement on the spent catalysts was carried out using a 200 kV G2 20 S-Twin Tecnai microscope. Energy dispersive X-ray spectroscopy (EDS) and high angle annular dark field scanning transmission electron microscopy (STEMHAADF) were performed on a Tecnai G2-F30 Field Emission Gun microscope. High Resolution TEM (HR-TEM) observations were carried out using a FEI TITAN3. Finally, XPS analyses of the spent catalytic samples presented herein were performed on a ThermoFisher Scientific Instruments.

### 2.3. Catalysts tests

The catalytic tests were performed at atmospheric pressure, using a continuous flow fixed bed tubular reactor. The gas mixture used as feed in the reactor inlet consisted of 55%  $\text{CH}_4$ , 35%  $\text{CO}_2$  and 10% Ar, corresponding to a  $\text{CH}_4/\text{CO}_2$  molar ratio equal to 1.56. The experimental protocol used was designed so as to investigate carbon deposition during the DRM reaction at different temperature as a function of time. Thus, the progress of the DRM reaction was investigated during short constant time-on-stream tests of 10 h, undertaken at different temperatures, at constant WHSV (40,000  $\text{mL g}^{-1} \text{h}^{-1}$ ). Reactants and products were analyzed on-line by gas chromatography in a CG-Agilent 7890A.

## 3. RESULTS AND DISCUSSION

### 3.1. Characterization results for spent catalysts

#### 3.1.1. Textural characterization

Figure 1 presents the  $\text{N}_2$  adsorption/desorption isotherms and the pore size distribution curves of the Ni/Al and Ni/modAl catalysts after reduction and after reaction at 600, 700 and 800°C. The isotherms for both samples are type IVa. The hysteresis loop for the Ni/Al reduced sample is type H2(b), which is characteristic of mesoporous materials. After reaction this loop was progressively

transformed to an H3 type, typical for materials with macropores. On the other hand, for the Ni/modAl samples (reduced and spent) the observed hysteresis loop is H3 type, as the adsorption branch resembles a Type II isotherm, and the lower limit of the desorption branch is normally located at the cavitation-induced  $P/P_0$ . The pore size distribution curves show that for the Ni/Al samples these are of single modal type in the mesopore range, centered around 10-20 nm with a shift to the micropore range for the sample used at 600 and 700 °C. On the contrary, for the Ni/modAl, the pore size distribution curves show that the majority of the population of pores is in the meso-range. It is noted that for the spent catalysts there is a shift to a larger mean diameter, indicating that a pore blocking exists at the meso-range. It is suggested that for both spent catalysts the carbon deposition occurring at the lower reaction temperatures (600 and 700 °C) covered the mesopores.

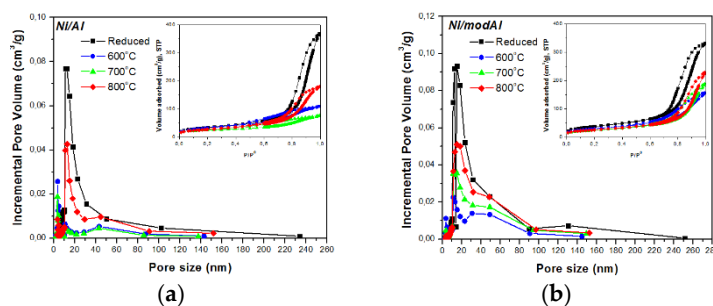


**Figure 1.** Pore size distribution and  $N_2$  adsorption-desorption isotherms (inset) of the reduced and spent catalysts at 600, 700 and 800 °C.

### 3.1.2. TGA/DTG analysis

The carbon deposited on to the spent catalysts tested herein was examined by TGA. It was observed that the oxidation process differed between the two samples. Specifically, for the Ni/Al the main thermal event was confined between 450 and 700 °C for the samples tested at 600 and 650 °C and expanded up to 800 °C for the samples tested at higher temperatures. In contrast, the main thermal event for the Ni/modAl catalyst was found between 450 and 800 °C. According to the literature, amorphous carbon combusts between 200-500 °C, disordered structures such as carbon nanofibers (CNFs) and carbon nanotubes (CNTs) with some defects and/or different structural arrangements are burned between 500 and 600 °C, and more graphitic structures, such as multi wall carbon nanotubes (MWCNTs) with an almost perfect graphene sheet arrangement combust between 600 and 800 °C [13]. Thus, amorphous, filamentous carbon and graphene-like structures were deposited on the catalysts during the reaction however higher fractions of graphitic structures were deposited on the Ni/Al, especially at higher reaction temperatures, as will be confirmed when discussing the Raman results below. Thus, it can be concluded that the addition of MgO and CaO on the alumina supporting material led to a less graphitic type of carbon, due to the higher rate of carbon oxidation, which could provide a catalyst with longer term stability.

### 3.1.3. Raman spectroscopy analysis

Raman spectroscopy was used to investigate the nature and the graphitization of the carbon deposited on the spent catalysts tested herein and the results are presented in Figure 2. Both samples show a first order region between 1000 and 2000  $cm^{-1}$  and a second order region between 2300 and 3300  $cm^{-1}$ . The first order region is governed by two broad bands, i.e., the G-band, which appears between 1500 and 1600  $cm^{-1}$ , and the D-band located between 1300 and 1400  $cm^{-1}$ . The deconvolution of the Raman spectra in all samples revealed that the G and D-band peaks were centered at 1565 and 1345  $cm^{-1}$  corresponding to CNTs. The degree of crystallinity of the carbon formed on the spent catalysts can be deduced by the relative intensity of the D and G-bands ( $I_D/I_G$ ), as smaller  $I_D/I_G$  values indicate higher crystallinity due to higher contribution of the graphitized carbon [14]. For the catalysts tested herein, it is clear that the degree of crystallinity increased with an increase of the reaction temperature however, this increase was significantly more pronounced for the Ni/Al catalyst. Specifically, the  $I_D/I_G$  ratio for the Ni/Al sample followed the order  $1.32 > 0.72 >$

0.45 > 0.44 > 0.35 and for the modified catalyst 1.42 > 1.18 > 1.06 > 0.98 > 0.86 at 600, 650, 700, 750 and 800 °C, respectively. Thus, the Raman spectra for the Ni/Al and Ni/modAl catalysts confirmed the formation of different carbon structures on the used catalysts.

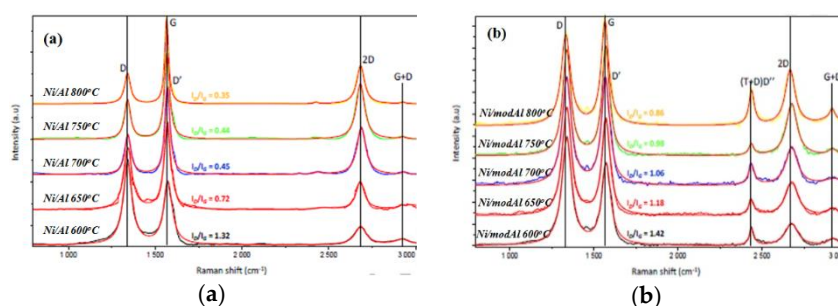


**Figure 2.** Pore size distribution and N<sub>2</sub> adsorption-desorption isotherms (inset) of the reduced and spent catalysts at 600, 700 and 800 °C.

### 3.1.4. Electron microscopy analysis

At 600 °C both samples exhibited crystalline carbon allotrope structures in the shape of carbon nanotubes, amorphous carbon and encapsulated Ni particles. At 800 °C, amorphous carbon was absent on the Ni/Al catalyst and encapsulated catalytic metallic nanoparticles could be observed. On the other hand, amorphous carbon could be observed on the modified system even after reaction at 800 °C [15]. Moreover, at 800 °C, the Ni/Al catalyst showed core-shell carbon coated Ni nanoparticles with highly graphitized CNTs formed, explaining the very low  $I_D/I_G$  ratios discussed above. From HR-TEM, a multitude of defects on the CNTs formed onto the Ni/modAl system could be observed. These defects are attributed to oxygen transferred and inserted in the graphitic lattice during CNT growth, which inhibits the formation of CNTs with continuous, straight walls and are important as they favour carbon oxidation.

### 3.3. Catalytic stability

The catalytic stability test results for the Ni/Al and Ni/modAl were conducted at different reaction temperatures (600, 650, 700, 750, 800 °C), using a fresh catalytic sample for each experiment. The variations in the values of XCH<sub>4</sub>, XCO<sub>2</sub> and YH<sub>2</sub> during reaction are depicted in Figure 3. For the Ni/Al sample a sharp drop in the conversion and yield values can be observed for the first two hours of the reaction (except at 800 °C), leading to a loss of about half of its initial activity. On the other hand, the Ni/modAl sample seems to deactivate at a more gradual rate and it appears to be more active and selective compared to the Ni/Al catalyst. The differences between the catalysts seem to be more pronounced at low reaction temperature and specifically at 650 °C, in which temperature the Ni/modAl catalyst has almost twice the values for both XCH<sub>4</sub> (40%) and YH<sub>2</sub> (35%) in comparison to the Ni/Al. Moreover, for both catalysts there is a decreasing trend to their final activity loss with an increase of the reaction temperature. Specifically, their activity loss ( $\Delta X(\text{CH}_4)\%$ ) ranges from 70% (600 °C) to 20% (800 °C) for the Ni/Al and from 50% (600 °C) to  $\approx 5\%$  (800 °C) for the Ni/modAl. It is noted that XCO<sub>2</sub>, YH<sub>2</sub>, YCO can be influenced by the RWGS reaction and only the XCH<sub>4</sub> stands as a true measure of the DRM activity. As for the H<sub>2</sub>/CO molar ratio, its values are almost constant in the time interval of the 10 h examined, except at the first 2 h of operation in which elevated H<sub>2</sub>/CO values (up to 1) were recorded. Elevated H<sub>2</sub>/CO values imply pronounced occurrence of the CH<sub>4</sub> cracking reaction, and/or Boudouard reaction, which are the main reactions responsible for carbon deposition. It should be mentioned that the catalysts underwent significant deactivation, due to the extremely severe experimental conditions that were applied, as an almost undiluted feed with a high CH<sub>4</sub> to CO<sub>2</sub> ratio (equal to 1.56) was used.

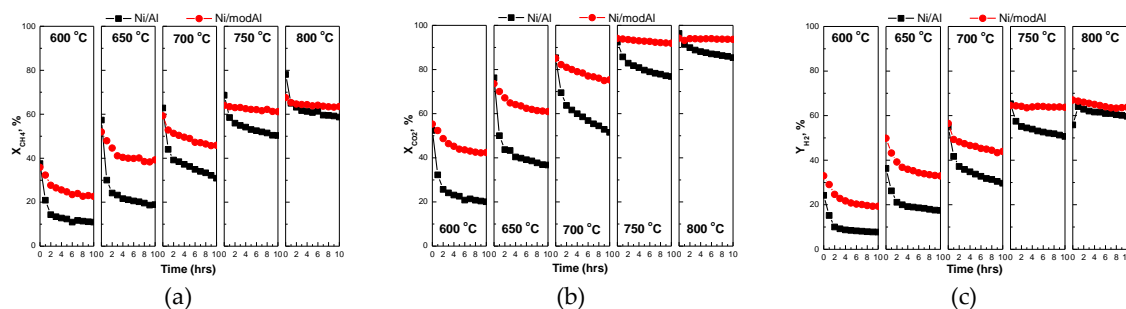


**Figure 3.** CH<sub>4</sub> and CO<sub>2</sub> conversion (%) for the Ni/Al and Ni/modAl catalysts for stability tests conducted at different temperatures.

#### 4. CONCLUSIONS

In the present work, the stability of Ni/Al and Ni/modAl catalysts was investigated for the biogas dry reforming reaction. The study focused on the correlation between deactivation and carbon deposition. In particular, for both spent catalysts, TGA and Raman results proved that the degree of carbon crystallinity increased with increasing the reaction temperature, whereas the addition of CaO and MgO led to a less graphitic type, which could actually provide a catalyst with longer term stability. Moreover, TEM analysis revealed that both samples presented graphitized carbon allotrope structures in the shape of carbon nanotubes, as well as co-existent amorphous carbon. The morphology of the carbon deposits demonstrated by the HR-TEM images showed clearly the defects of the CNTs formed onto the spent Ni/modAl catalyst. Stability tests confirmed that the modified catalyst deactivated at a more gradual rate and was more active and selective in comparison to the Ni/Al for all reaction temperatures. Specifically, Ni/modAl exhibited good durability in terms of CH<sub>4</sub> conversion and H<sub>2</sub> selectivity, whereas the Ni/Al gradually lost its activity in CH<sub>4</sub> conversion with a concomitant decrease of the H<sub>2</sub> yield. It can be concluded that the doping of Al<sub>2</sub>O<sub>3</sub> with CaO and MgO stabilized the catalyst by: (a) maintaining the Ni<sup>0</sup> phase during the reaction, due to higher dispersion and stronger active phase-support interactions and (b) improved the deposited carbon gasification by the Reverse Boudouard reaction due to the enhanced CO<sub>2</sub> adsorption on its increased surface basic sites.

**Author Contributions:** Conceptualization, NDC; Data curation, GIS, VS, SJH, VGP, WW; Formal analysis, NDC, GIS, MAB, KP; Funding acquisition, MAG, VGP, WW; Methodology, NDC; Project administration, NDC, MAG; Project coordination, MAG; Resources, MAG; Supervision, NDC; Writing—original draft, GIS; Writing—review & editing, NDC, MAB, KP, MAG; All authors have read and agreed to the published version of the manuscript.

**Acknowledgments:** This research has been co-financed by the European Union and Greek national funds under the call “Greece – China Call for Proposals for Joint RT&D Projects” (Project code: T7DKI-00388).

**Conflicts of Interest:** The authors declare no conflict of interest.

#### References

- Goula, M.A.; Charisiou, N.D.; Papageridis, K.N.; Delimitis, A.; Pachatouridou, E.; Iliopoulou, E.F. Nickel on alumina catalysts for the production of hydrogen rich mixtures via the biogas dry reforming reaction: influence of the synthesis method. *Int. J. Hydrogen Energy* **2015**, *40*, 9183–9200.
- Charisiou, N.D.; Siakavelas, G.; Papageridis, K.N.; Baklavaridis, A.; Tzounis, L.; Avraam, D.G.; Goula, M.A. Syngas production via the biogas dry reforming reaction over nickel supported on modified with CeO<sub>2</sub> and/or La<sub>2</sub>O<sub>3</sub> alumina catalysts. *J. Nat. Gas Sci. Eng.* **2016**, *31*, 164–183.
- Goula, M.A.; Charisiou, N.D.; Siakavelas, G.; Tzounis, L.; Tsiaoussis, I.; Panagiotopoulou, P.; Goula, G.; Yentekakis, I.V. Syngas production via the biogas dry reforming reaction over Ni supported on zirconia modified with CeO<sub>2</sub> or La<sub>2</sub>O<sub>3</sub> catalysts. *Int. J. Hydrogen Energy* **2017**, *42*, 13724–13740.
- Italiano, C.; Balzarotti, R.; Vita, A.; Latorrata, S.; Fabiano, C.; Pino, L.; Cristiani, C. Preparation of structured catalysts with Ni and Ni-Rh/CeO<sub>2</sub> catalytic layers for syngas production by biogas reforming processes. *Catal. Today* **2016**, *273*, 3–11.

5. Juan-Juan, J.; Roman-Martinez, M.C.; Illan-Gomez, M.J. Nickel catalyst activation in the carbon dioxide reforming of methane: effect of pretreatments. *Appl. Catal. A-Gen* **2009**, *355*, 27-32.
6. Montoya, J.A.; Romero-Pascual, E.; Gimon, C.; Del Angel, P.; Monzon A. Methane reforming with CO<sub>2</sub> over Ni/ZrO<sub>2</sub>-CeO<sub>2</sub> catalysts prepared by sol-gel. *Catal. Today* **2000**, *63*, 71-85.
7. Zhan, Y.; Han, J.; Bao, Z.; Cao, B.; Li, Y.; Street, J.; Yu, F. Recent advances in dry reforming of methane over Ni-based catalysts. *Mol. Catal.* **2017**, *436*, 248-258.
8. Kathiraser, Y.; Wang, Z.; Ang, M.L.; Mo, L.; Li, Z.; Oemar, U.; Kawi, S. Highly active and coke resistant Ni/SiO<sub>2</sub> catalysts for oxidative reforming of model biogas: effect of low ceria loading. *J. CO<sub>2</sub> Util.* **2017**, *19*, 284-295.
9. Vasiliades, M.A.; Makri, M.M.; Djinovic, P.; Erjavec, B.; Pintar, A.; Efstathiou, A.M. Dry reforming of methane over 5wt% Ni/Ce<sub>1-x</sub>Pr<sub>x</sub>O<sub>2-δ</sub> catalysts: performance and characterisation of active and inactive carbon by transient isotopic techniques. *Appl. Catal. B-Environ* **2016**, *197*, 168-183.
10. Bellido, J.D.A.; Assaf, E.M. Effect of the Y<sub>2</sub>O<sub>3</sub>-ZrO<sub>2</sub> support composition on nickel catalyst evaluated in dry reforming of methane. *Appl. Catal. A-Gen* **2009**, *352*, 179-187.
11. Rezaei, M.; Alavi, S.M.; Sahebdehfar, S.; Yan, Z.-F. Effects of K<sub>2</sub>O promoter on the activity and stability of nickel catalysts supported on mesoporous nanocrystalline zirconia in CH<sub>4</sub> reforming with CO<sub>2</sub>. *Energy Fuel* **2008**, *22*, 2195-2202.
12. Charisiou, N.D.; Papageridis, K.N.; Tzounis, L.; Sebastian, V.; Baker, M.A.; Hinder, S.J.; AlKetbi, M.; Polychronopoulou, K.; Goula, M.A. Ni supported on CaO-MgO-Al<sub>2</sub>O<sub>3</sub> as a highly selective and stable catalyst for H<sub>2</sub> production via the glycerol steam reforming reaction. *Int. J. Hydrogen Energy* **2019**, *44*, 256-273.
13. Velasquez, M.; Batiot-Dupeyrat, C.; Gallego, L.; Santamaria A. Chemical and morphological characterization of multi-walled-carbon nanotubes synthesized by carbon deposition from an ethanol-glycerol blend. *Diam. Relat. Mater.* **2014**, *50*, 38-48.
14. Awadallah, A.E.; Aboul-Enein, A.A.; El-Desouki, D.S.; Aboul-Gheit, A.K. Catalytic thermal decomposition of methane to CO<sub>x</sub>-free hydrogen and carbon nanotubes over MgO supported bimetallic group VIII catalysts. *Appl. Surf. Sci.* **2014**, *296*, 100-107.
15. Sutthumporn, K.; Kawi, S. Promotional effect of alkaline earth over Ni-La<sub>2</sub>O<sub>3</sub> catalyst for CO<sub>2</sub> reforming of CH<sub>4</sub>: role of surface oxygen species on H<sub>2</sub> production and carbon suppression. *Int. J. Hydrogen Energy* **2011**, *36*, 14435-14446.

